



LUND UNIVERSITY

Comparison of photo detectors and operating conditions for decay time determination in phosphor thermometry

Knappe, Christoph; Abou Nada, Fahd Jouda; Richter, Mattias; Aldén, Marcus

Published in:
Review of Scientific Instruments

DOI:
[10.1063/1.4746990](https://doi.org/10.1063/1.4746990)

2012

[Link to publication](#)

Citation for published version (APA):
Knappe, C., Abou Nada, F. J., Richter, M., & Aldén, M. (2012). Comparison of photo detectors and operating conditions for decay time determination in phosphor thermometry. *Review of Scientific Instruments*, 83(9), Article 094901. <https://doi.org/10.1063/1.4746990>

Total number of authors:
4

General rights

Unless other specific re-use rights are stated the following general rights apply:
Copyright and moral rights for the publications made accessible in the public portal are retained by the authors and/or other copyright owners and it is a condition of accessing publications that users recognise and abide by the legal requirements associated with these rights.

- Users may download and print one copy of any publication from the public portal for the purpose of private study or research.
- You may not further distribute the material or use it for any profit-making activity or commercial gain
- You may freely distribute the URL identifying the publication in the public portal

Read more about Creative commons licenses: <https://creativecommons.org/licenses/>

Take down policy

If you believe that this document breaches copyright please contact us providing details, and we will remove access to the work immediately and investigate your claim.

LUND UNIVERSITY

PO Box 117
221 00 Lund
+46 46-222 00 00

Comparison of photo detectors and operating conditions for decay time determination in phosphor thermometry

C. Knappe, F. Abou Nada, M. Richter, and M. Aldén

Citation: [Rev. Sci. Instrum.](#) **83**, 094901 (2012); doi: 10.1063/1.4746990

View online: <http://dx.doi.org/10.1063/1.4746990>

View Table of Contents: <http://rsi.aip.org/resource/1/RSINAK/v83/i9>

Published by the [American Institute of Physics](#).

Related Articles

High resolution resistive thermometry for micro/nanoscale measurements

[Rev. Sci. Instrum.](#) **83**, 084902 (2012)

Safe and consistent method of spot-welding platinum thermocouple wires and foils for high temperature measurements

[Rev. Sci. Instrum.](#) **83**, 084901 (2012)

Printable tiny thermocouple by liquid metal gallium and its matching metal

[Appl. Phys. Lett.](#) **101**, 073511 (2012)

Metallic Coulomb blockade thermometry down to 10 mK and below

[Rev. Sci. Instrum.](#) **83**, 083903 (2012)

Perpendicular-flow, single-wafer atomic layer deposition reactor chamber design for use with in situ diagnostics

[Rev. Sci. Instrum.](#) **83**, 083106 (2012)

Additional information on Rev. Sci. Instrum.

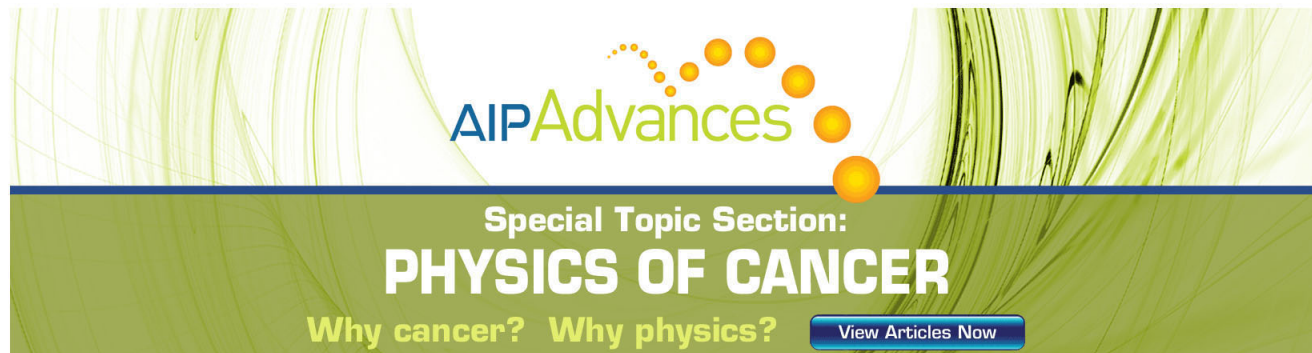
Journal Homepage: <http://rsi.aip.org>

Journal Information: http://rsi.aip.org/about/about_the_journal

Top downloads: http://rsi.aip.org/features/most_downloaded

Information for Authors: <http://rsi.aip.org/authors>

ADVERTISEMENT

The advertisement features a green and yellow abstract background with flowing lines. At the top, the 'AIP Advances' logo is displayed, with 'AIP' in blue and 'Advances' in green, accompanied by a series of orange dots of varying sizes. Below the logo, the text 'Special Topic Section: PHYSICS OF CANCER' is written in white, with 'PHYSICS OF CANCER' in a larger, bold font. At the bottom, the phrase 'Why cancer? Why physics?' is written in yellow, and a blue button with the text 'View Articles Now' is positioned on the right.

AIP Advances

Special Topic Section:
PHYSICS OF CANCER

Why cancer? Why physics? [View Articles Now](#)

Comparison of photo detectors and operating conditions for decay time determination in phosphor thermometry

C. Knappe, F. Abou Nada, M. Richter, and M. Aldén

Division of Combustion Physics, Lund University, Box 118, SE-221 00 Lund, Sweden

(Received 5 June 2012; accepted 4 August 2012; published online 5 September 2012)

This work compares the extent of linear response regions from standard time-resolving optical detectors for phosphor thermometry. Different types of photomultipliers (ordinary and time-gated) as well as an avalanche photodiode were tested and compared using the phosphorescence decay time of cadmium tungstate (CdWO_4). Effects originating from incipient detector saturation are revealed as a change in evaluated phosphorescence decay time, which was found to be a more sensitive measure for saturation than the conventional signal strength comparison between in- and output. Since the decay time of thermographic phosphors is used for temperature determination systematic temperature errors in the order of several tens of Kelvins may be introduced. Saturation from the initial intensity is isolated from temporally developed saturation by varying the CdWO_4 decay time over the microsecond to nanosecond range, resultant of varying the temperature from 290 to 580 K. A detector mapping procedure is developed in order to identify linear response regions where the decay-to-temperature evaluations are unbiased. In addition, this mapping procedure generates a library of the degree of distortion for operating points outside of linear response regions. Signals collected in the partly saturated regime can thus be corrected to their unbiased value using this library, extending the usable detector operating range significantly. © 2012 American Institute of Physics. [<http://dx.doi.org/10.1063/1.4746990>]

I. INTRODUCTION

Phosphors are ceramic materials that exhibit an extended afterglow after being optically excited. A phosphor is thermographic when the phosphorescent light emission varies as a function of temperature. Both the changes in phosphorescence decay as well as the intensity ratio of different optical regions in the emission spectra can be exploited for thermometry.^{1–3}

As the decay time of a phosphor can change several orders of magnitude for a given temperature range, point measurements exploiting the time decay are often preferred over intensity-ratio based methods when high temperature precision is demanded. Consequently, recent attempts pushed the decay-time retrieval towards 2D application by either using a stack of sequentially gated CCD cameras⁴ or fast framing CMOS devices.⁵

Measurement precision and accuracy in phosphor thermometry highly depends on the phosphor itself, its sensitivity to temperature changes and whether phosphorescence is affected by other interfering factors such as pressure,⁶ ambient gas composition⁷ or the post growth process of annealing.^{8–10} In some applications the layer thickness of the phosphor may contribute as a substantial source of error¹¹ and also multi-exponential decays can introduce ambiguities to the retrieval of a distinct temperature.¹²

Apart from phosphor characteristics, there are other factors to consider that restrict the accuracy of phosphor thermometry. For obvious reasons, the reliability of the temperature calibration is a key feature, i.e., how well is the temperature known during calibration, how many calibration points are sufficient for a given temperature interval and whether the same decay time can be reproduced for a set of different sig-

nal intensities. The latter question is a matter of light detection and is aimed to be addressed in this paper. Previous studies have shown that detector saturation might introduce substantial systematic errors to the signal evaluation process in phosphor thermometry.^{13,14} This work seeks to compare the performance of four different standard detectors under identical test conditions. Each detector was exposed to the phosphorescence of cadmium tungstate (CdWO_4) at five different temperatures under varying light intensities and detector gains.

II. EXPERIMENTAL

A. Selection of detectors

Four time-resolving point detectors have been chosen for comparison within this study. The selection consists of two different photomultiplier tubes (PMTs), a multi-channel plate photomultiplier tube (MCP-PMT) and a fiber-coupled avalanche photodiode (APD). One of the two PMTs can optionally be run in time-gated mode and also offers a more sensitive photocathode within the investigated wavelength range around 450 nm. The MCP-PMT could only be used in time-gated mode. However, by triggering the PMT-gate to open either 10 ns before or after the first phosphorescence photons hit the detector allowed to study the impact of an initial peak on the signal shape. Signal outputs from all detection devices were either directly coupled to a 350 MHz digital oscilloscope using an input resistance of 50 Ω , or optionally connected to an in-house made external current-to-voltage amplifier (5 MHz bandwidth). In total, seven different detector configurations were tested as listed in Table I. The gain column below represents the electrical amplification

TABLE I. Detectors and tested operating modes.

Detector type	Specific name	Mode of operation	Gain range
PMT1	H6780-04	Continuous	480–43000
PMT1	H6780-04	Cont. + amplified	42–80
PMT2	H11526-20-NF	Continuous	950–7700
PMT2	H11526-20-NF	Time-gated: +10 ns	950–7700
MCP-PMT	R5916U-50	Time-gated: –10 ns	36–3000
MCP-PMT	R5916U-50	Time-gated: +10 ns	36–3000
APD	S5343	Continuous	62–470

range that was investigated for each detector. It has been defined according to oscilloscope peak voltages ranging from less than 100 mV up to a few Volts for each temperature and detector. Maximum peak voltages varied to some degree from detector to detector due to their different specified output current limits.

B. Experimental setup

Figure 1 displays the experimental setup, which was used to compare all detectors in their individual modes of operation (see Table I). A 10 Hz pulsed Nd:YAG laser, operating at 266 nm was used as an excitation source for CdWO₄, that was placed in a tube furnace. CdWO₄ was chosen, in particular, as it emits strong- and almost single-exponential phosphorescence light, without suffering from irreversible emission changes when exposed to elevated temperatures below 600 K. Its broadband emission centered around 470 nm is temperature sensitive from room temperature up to around 580 K, offering a vast range of decay times that span from 10 μ s down to less than 10 ns.

The phosphorescence was imaged onto the detector by a 300 mm quartz lens at a 90° angle to the laser path axis. A combination of a >400 nm transmission edge filter and a 450 nm bandpass filter (FWHM = 40 nm) was placed in front of the detector to suppress spurious laser radiation and to spectrally isolate the phosphorescence emission.

Two identical PMTs (H6780-04, same type as PMT1 in Table I) were added to the setup in Figure 1 for the purpose of

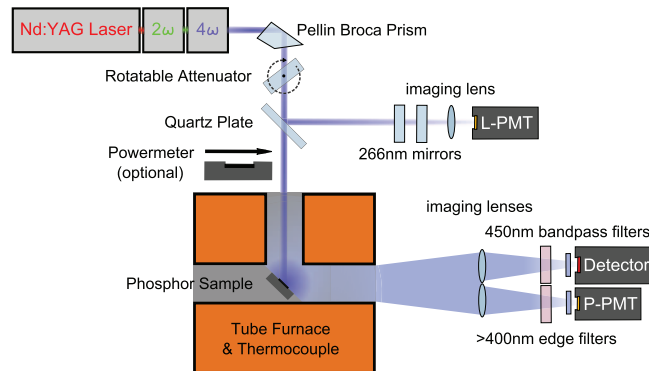


FIG. 1. Experimental setup for testing the temporal performance of a detector as a function of light intensity, gain and temperature. L- and P-PMT are two identical PMTs referencing the amount of impinging photons per time interval after being calibrated against the power meter.

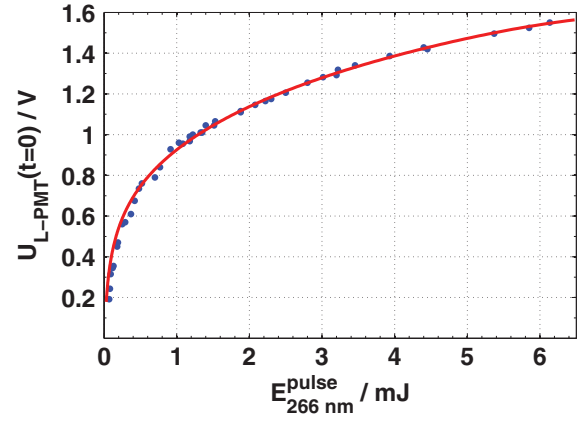


FIG. 2. Fitted correlation (red line) showing the signal peak voltage from L-PMT in as a function of Laser pulse energy. The gain of the L-PMT was set to a constant value of 6300 and additional transmission losses T_{L-PMT} were introduced (see Figure 1) in order to prevent detector damage.

monitoring the phosphor's response to laser intensity changes. Keeping track on the phosphor behavior is important in order to monitor any possible phosphor-intrinsic decay-time dependence on laser irradiance (see Ref. 10) that might superpose with detector-specific results. The detector denoted as L-PMT monitors the laser pulse-to-pulse fluctuations. Once calibrated against a powermeter, it serves as a reference for the laser pulse energy, see Figure 2.

Henceforth, the laser pulse energy $E_{266 nm}^{pulse}$ can be described as a function of the L-PMT peak voltage $U_{L-PMT}(t=0)$ using the following fitted relation:

$$E_{266 nm}^{pulse} = F[U_{L-PMT}(t=0)] = a(e^{b \cdot U_{L-PMT}(t=0)} - 1). \quad (1)$$

The fitting constants in Eq. (1) have been obtained by a Levenberg-Marquardt fitting algorithm and are given by $a = (90 \pm 4) \mu$ J and $b = (2.76 \pm 0.03) \text{ V}^{-1}$. The inverse relation of (1), i.e., $U_{L-PMT}(t=0) = F^{-1}(E_{266 nm}^{pulse})$ is represented by a red line in Figure 2 and clearly shows a saturated behavior of the reference PMT from an early stage on.

The other reference PMT in Figure 1 (P-PMT) was placed behind identical optics as the currently investigated detector to serve as a reference for the incoming amount of light, assuming that phosphorescence was emitted isotropically from the phosphor target. Both L- and P-PMT were set to an identical gain of 6300 and relative transmission losses $T_{L-PMT} (\approx 10^{-7})$ were introduced towards the laser reference in order to ensure similar peak output voltages for both references at all times.

C. Operating conditions

The total amount of phosphorescent light emitted per excitation event is a function of initial signal intensity I_0 and the phosphorescence decay time τ . It can be sufficiently described by integrating over the time-dependent phosphorescence intensity I , described by Eq. (2),

$$I = I_0 \cdot \exp\left(-\frac{t}{\tau}\right). \quad (2)$$

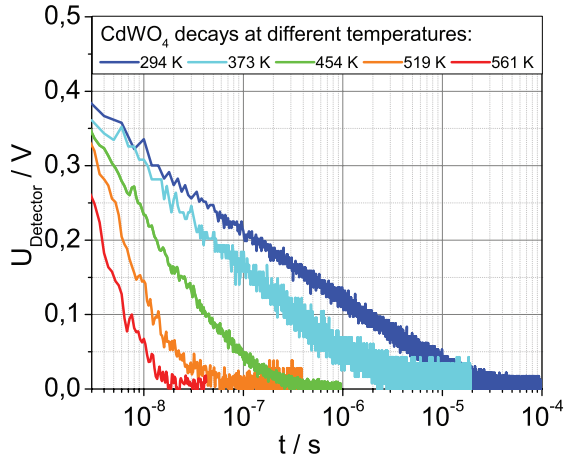


FIG. 3. Phosphorescence decay curves from CdWO₄ displayed at five different temperatures. As every detector yielded slightly different decay times, τ values are not explicitly given here but can be found in Figure 17 instead.

It follows that detector saturation caused by incident light is dependent on both I_0 and τ , hence, the detector response would not only be altered by irradiances above a certain threshold ($I_0 > I_{\text{thresh}}$), but also by the time ($\sim \tau$) that the detector is exposed to elevated light intensities.

For this reason, I_0 and τ have been investigated independently by repeating each gain- and intensity variation experiment for a number of fixed phosphorescence decay times. Every detector listed in Table I was exposed to phosphorescence from a phosphor coated target kept at five specific temperatures in the tube furnace: 294, 373, 454, 519, and 561 K. Temperatures were measured using a K-type thermocouple (attached to the phosphor-coated target) and chosen such that there was a reasonable step size for the decay time in between two proximate temperatures, see Figure 3.

In order to address I_0 the authors decided to estimate the amount of photons, $N_{\lambda}^{\text{P-PMT}}[U_{\text{P-PMT}}(t=0)]$, reaching the detector within a time window of $\Delta t = 1$ ns, using the reference voltage from the P-PMT and the energy calibration from (1). The center of this time window coincides with the registered signal peak value of the phosphorescence curve ($t = 0$), as seen in Figure 4.

The laser pulse profile in Figure 4 is essentially a Gaussian function with a full width half maximum (FWHM) of fitted to be 7.46 ns. This is slightly broader compared to the laser manufacturer specification value of 6 ns because the reference detectors are partly saturated and have a limited signal rise time of 750 ps. Taking into account the radiant photocathode sensitivity being a function of wavelength λ ($S_{450 \text{ nm}}/S_{266 \text{ nm}} \approx 1.23$, see Ref. 15), the number of phosphorescence photons $N_{\lambda}^{\text{P-PMT}}$ arriving at $t = (0 \pm 0.5)$ ns can be estimated by Eq. (3):

$$N_{\lambda}^{\text{P-PMT}}[U_{\text{P-PMT}}(t=0)] \approx \frac{S_{266 \text{ nm}}}{S_{\lambda}} \cdot 2\sqrt{\frac{\ln 2}{\pi}} \cdot \frac{F[U_{\text{P-PMT}}(t=0)]}{E_{\lambda}^{\text{photon}}} \cdot \frac{\Delta t}{\text{FWHM}} \cdot T_{\text{L-PMT}}. \quad (3)$$

The Appendix covers a derivation of Eq. (3) as well as an error estimation for $N_{\lambda}^{\text{P-PMT}}$.

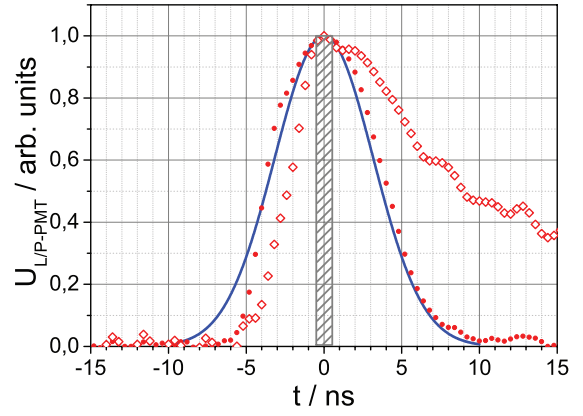


FIG. 4. Normalized signal profiles for both reference PMTs as a function of time. A Gaussian (solid blue line) has been plotted to illustrate similarities to the laser profile, expressed as solid red dots recorded by the L-PMT. The corresponding phosphorescence time response recorded by the P-PMT is represented by red hollow diamonds. A shaded box with a width of 1 ns has been centered on the signal maximum at $t = 0$.

As the laser energy is scanned from 15 μJ to 5 mJ using an adjustable attenuator (see Figure 1), the phosphorescence intensity changes proportionally allowing the investigation of each detector's response to various intensities at several gain settings (see Table I). Figure 5 supports this approach as it shows a largely linear relation between the laser energy (\sim L-PMT signal) and phosphorescence signal (P-PMT) due to the fact that both reference detectors saturate similarly. However, some minor deviations from linearity can be observed at low laser energies.

III. RESULTS AND DISCUSSION

The phosphorescence decay time was evaluated based on a least squares fit algorithm (Levenberg-Marquardt) to a single-exponential function, see Eq. (1). To avoid contributions from changing fitting window positions to the evaluated results, a fixed evaluation time window was chosen for each temperature. However, the window size was adapted

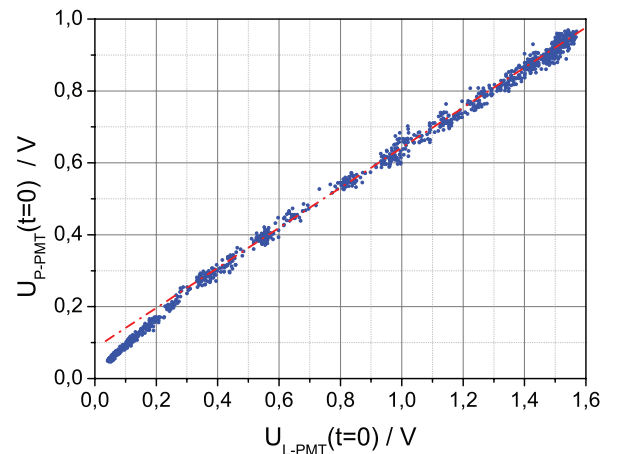


FIG. 5. Reference PMT peak signal voltages at gain 6300 corresponding to a full laser excitation energy scan from 15 μJ to 5 mJ at room temperature.

TABLE II. Fitting time window positions after the initial signal peak as a function of temperature.

Temperature / K	Start / s	Stop / s
294	10^{-8}	5×10^{-5}
373	10^{-8}	1×10^{-5}
454	10^{-8}	8×10^{-7}
519	10^{-8}	1.5×10^{-7}
561	10^{-8}	8×10^{-8}

according to the temperature in order to capture large parts of the decay, see Table II.

One exception from Table II has been made for the case of external current-to-voltage amplification: Due to the limited bandwidth of the amplifier the start of the evaluation window was set to 60 ns instead of 10 ns.

For obvious reasons, the recorded phosphorescence decay time is a measure of the time-distribution of the detector output signal: An ideal optical detector having a linear response should reproduce similar signal shapes leading to constant decay times, regardless the amount of incident light or the extent of internal signal amplification. This ideal case, however, is often far from reality as the authors have shown in Ref. 14. Two normalized decay curves displayed in Figure 6 have been measured from the same phosphorescence signal at room temperature using two different gain settings for the detector. Within the same observation window the evaluated decay time from PMT1 varied from 11 μ s to 23 μ s, i.e., more than a factor of two due to a change in detector gain. This behavior is supported by Figure 2, which indicated the non-linear signal response of a similar PMT during laser energy calibration.

Figure 7 illustrates how the evaluated decay time varies as a function of gain setting and phosphorescence intensity at constant temperature. It has been produced without using the reference PMTs and displays the detector peak voltage $U_{\text{Detector}}(t=0)$ instead of photon number on the x axis. The phosphorescence has been varied within the same intensity range for each detector gain. Also, the y axis displays the gain

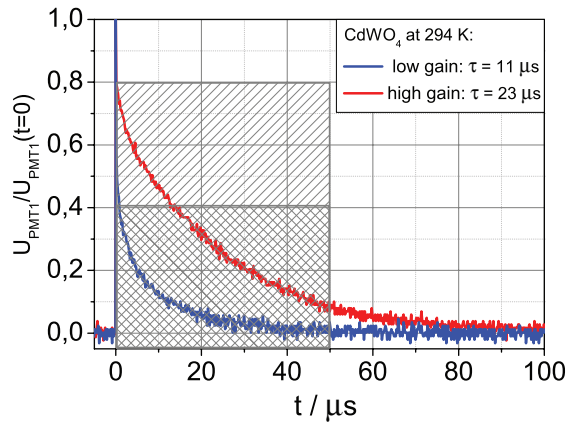


FIG. 6. Normalized time response of CdWO₄ phosphorescence, observed at 294 K by PMT1 using two different gain settings. The decay-time observation window for each curve has been indicated by the shaded boxes according to Table II.

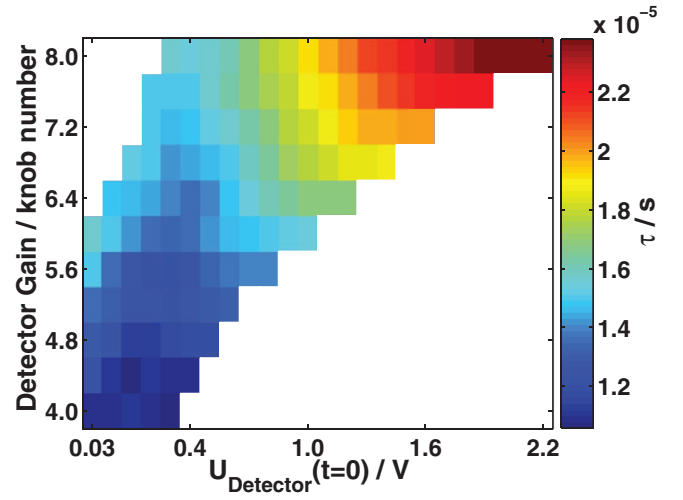


FIG. 7. Decay-time response surface of PMT1 at 294 K, shown in its original axes, gain knob number and detector peak voltage.

readout value as arbitrary unit “knob number” and translates into the control voltage for the detector. Using data sheets provided by the manufacturers (see Ref. 15), this control voltage has been converted into actual gain values later on to allow a more general gain comparison between different detectors. $U_{\text{Detector}}(t=0)$ is dependent on both incident light flux and detector gain, leaving large matrix parts empty in Figure 7. It is thus impossible to distinguish effects from gain and incident light on the detected decay time from this plot. However, Figure 7 offers the clear advantage of showing actual reading values, allowing the experimenter to judge stability towards changes in operating condition while performing measurements. It is interesting to note that varying signal intensities in experiments cannot be compensated by changing the detector gain without affecting the decay signal shape. This comes clear when following a constant peak voltage across several gain columns with respect to the decay time, for example at $U_{\text{Detector}}(t=0) = 0.3$ V.

Figure 8 shows the detector response surface for PMT1 at 373 K, now displayed as a function of gain and photon number according to Eq. (3). The evaluated decay time is

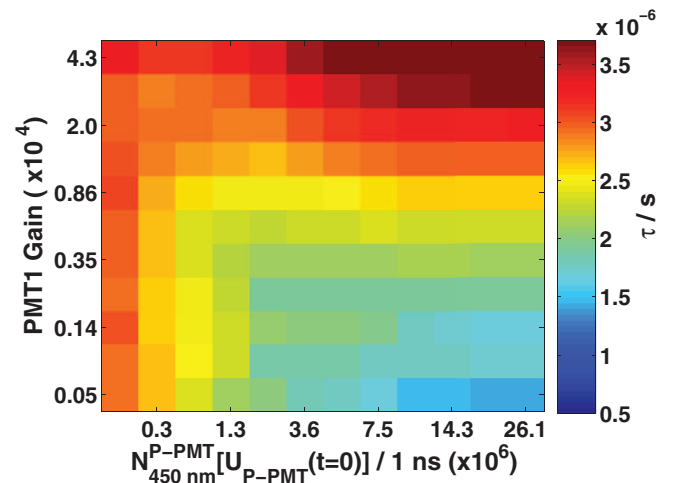


FIG. 8. Response surface of PMT1 at 373 K.

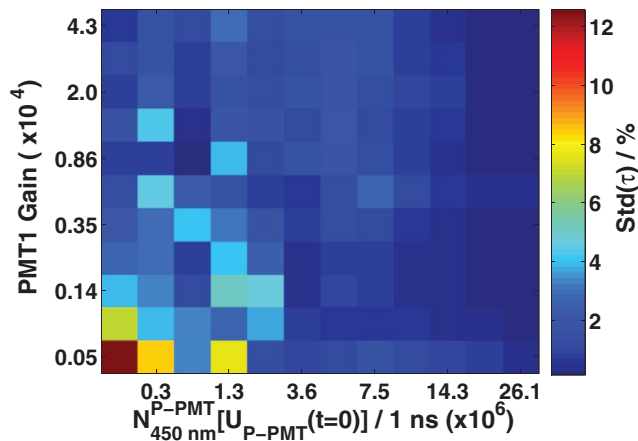


FIG. 9. Decay time standard deviation at 373 K using PMT1, normalized by the value of each matrix element in Figure 8.

represented by a color scale as a function of gain and photon impingement within 1 ns at signal peak levels. Every matrix element contains contributions of 10–500 single decays, each evaluated individually before averaging. In the upper right region at high gains and photon numbers the evaluated decays are longer. As this behavior changes with gain, it can be identified as a detector artifact, caused by saturation. The lower right area in Figure 8 has a rather constant decay-time distribution, which is desirable for phosphorescence measurements. For low light exposures, there is a lifetime gradient visible that is gain-independent. It will be discussed in the context of further findings later on.

Figure 9 provides information on the measurement precision within this study. It shows the decay time standard deviation of the response matrix in Figure 8 normalized by each individual pixel average. Except for the lower left corner in Figure 9, where weak signals were recorded due to low light intensities and gains, the standard variation is well below 5%. It indicates the results to be reproducible to a large degree, which has also been confirmed by direct comparison with repeated measurements.

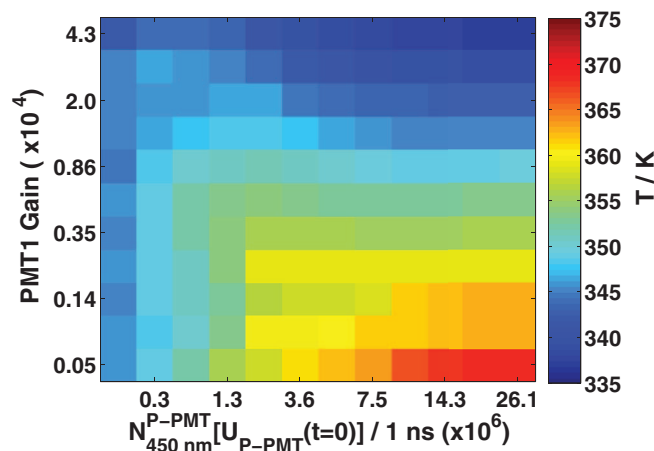


FIG. 10. Artificial temperatures, calculated from Figure 8 using previous temperature calibration data. The actual phosphor temperature was kept constant at 373 K.

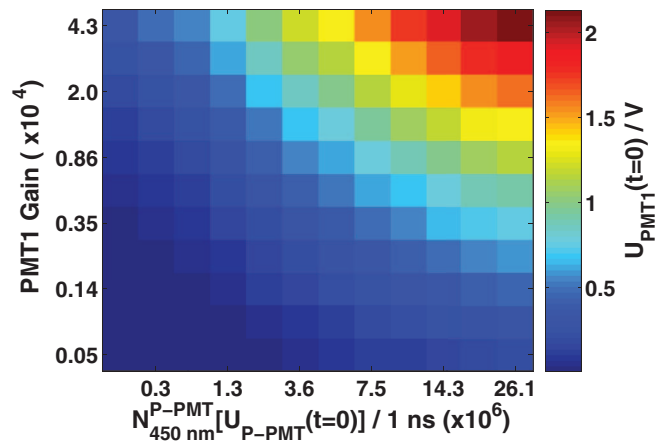


FIG. 11. Detector peak voltage of PMT1 during gain/intensity response tests at 373 K.

Figure 10 uses a temperature calibration of CdWO_4 , produced within a previous study (see Ref. 14) in order to calculate artificial temperatures from the detector matrix in Figure 8. It should be highlighted at this point, that all measurement data from Figure 10 has been acquired at a constant temperature of 373 K and that the temperature distribution shown is a consequence of nonlinear measurement response. The temperature distribution observed from Figure 10 spans across 40 K, which represents more than 13% of the phosphor's original temperature sensitivity range. Furthermore, CdWO_4 has a decay-time characteristic that changes 3 orders of magnitude within a temperature interval of merely 300 K. Since artificial temperatures, retrieved by temperature calibration curves highly depend on the sensitivity of the phosphor, it should be noted that most other phosphors are less sensitive than CdWO_4 and will thus exhibit an even higher spread of artificial temperatures.

Figure 11 displays the detector peak voltage of PMT1 during the acquisition of a response matrix at 373 K (see Figure 8). The signal peak voltage reaches a maximum of 2 V in the upper right corner of the plot. However, more than half the data points from Figure 11 were derived from signals with peak voltages of 500 mV or below, i.e., output values that previously in Figure 2 seemed to correspond to a linear detector response. In contrast, Figures 8 and 10 indicate vast decay-time gradients from these regions demonstrating superior sensitivity for highlighting detector nonlinearities.

Figure 12 shows the same detector arrangement as in Figure 8, now tested at 561 K. Lower phosphorescence quantum yields at elevated temperatures caused the last photon number column to be empty. The two elements that made an exception contain just a single decay each, caused by random laser fluctuation. Also the area of saturation in the upper right corner retreated to some extent, which is likely to be caused by shorter decays limiting the space charge build-up time at the end of the dynode chain.^{16–18} The lifetime gradient for low light intensities (present in Figure 8) has vanished and some elements at low gains and intensities remained empty due to signal-to-noise (S/N) issues at shorter decays.

In Figure 13 another PMT (PMT2) was exposed to phosphorescence radiation at 373 K. The gain range was

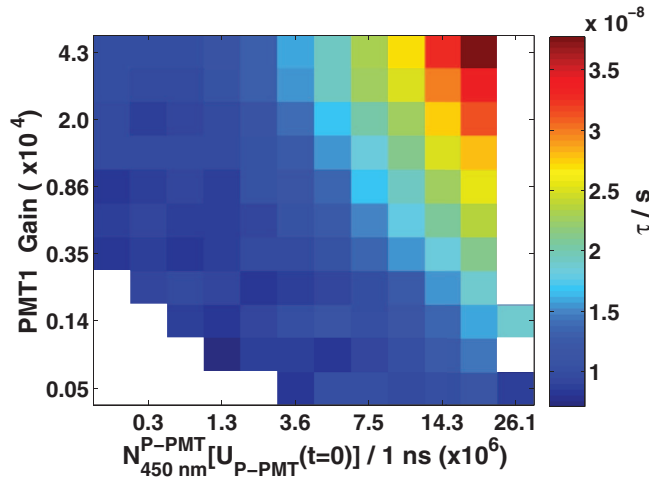


FIG. 12. Response surface of PMT1 at 561 K.

chosen smaller this time in order to limit signal output currents. PMT2 had a significantly higher sensitivity around 450 nm compared to PMT1. The upper gain region ended at 7700, which is where PMT1 in Figure 8 still was not influenced by the saturated region of high gain and intensity. In accordance to these results, Figure 13 does not show any saturation limits for the high signal regions, which makes it a preferable device for phosphor thermometry in comparison to PMT1.

However, the lifetime gradient for the low light level region is still present and stretches across the same range of intensities as observed with PMT1, i.e., for excitation energies lower than 30 μJ (peak phosphorescence $< 1.3 \times 10^6$ photons/ns). This might suggest the phosphor as a possible cause, which is supported by the deviation from a linear relation at low laser energies between the two reference PMTs in Figure 5. Moreover, similar findings have been reported by Ref. 10, showing the phosphorescence decay time of another phosphor, $\text{Mg}_4\text{FGeO}_6\text{:Mn}$, decreasing for increasing laser excitation energies. PMT2 has another advantage, which is being capable of operating in time-gated mode. This enables suppression of fluorescence peaks that might superimpose with incipient phosphorescence, allowing

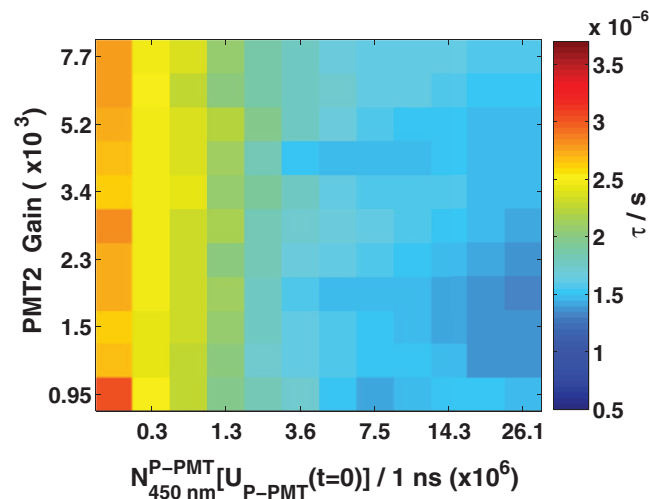


FIG. 13. Response surface of PMT2 at 373 K.

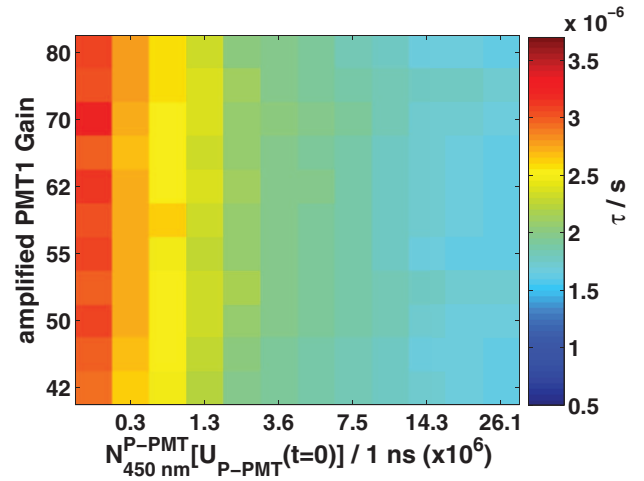


FIG. 14. Response surface of PMT1 (amplified) recorded at 373 K.

a more efficient utilization of the dynamic output range.¹⁴ Since the saturated region was not reached during experiments with PMT2, time-gated results showed very little variation to the presented plots.

Using PMT1 together with the external current-to-voltage amplifier resulted in reasonable signal levels at much lower PMT gain settings, but came at the cost of reduced temporal resolution. This helps avoiding detector saturation as seen in Figure 14, but also bandwidth-limits the retrieval of shorter decays, i.e., the amplifier confines the detection limit at high temperatures rather than the phosphor.

Figure 15 presents the detector response surface of the MCP-PMT at 373 K, with the gate opening 10 ns prior to the phosphorescence onset. Even though output currents have been four times higher for the MCP-PMT compared to PMT1 (Figure 8), this device seems not to be affected by high signal saturation. Therefore, cutting off the first intense part of the phosphorescence by triggering the gate to open 10 ns after the signal's peak voltage did not show a significant difference.

Finally, Figure 16 displays decay-time results, accumulated by using the APD at 373 K. A significant amount of data for the low light intensities has been rejected by the

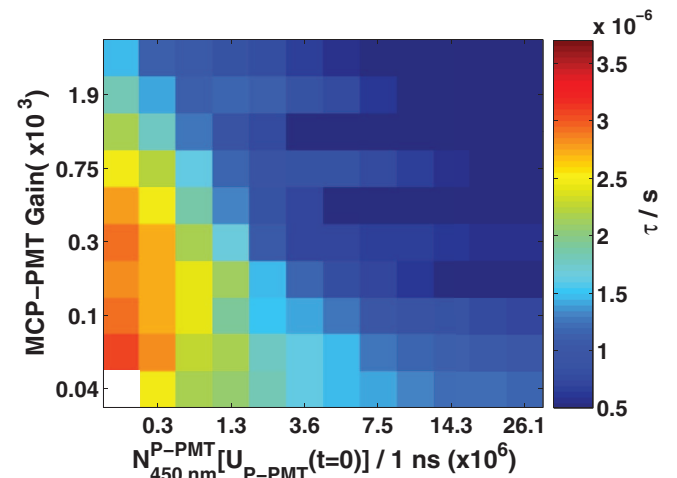


FIG. 15. Response surface of MCP-PMT at 373 K, triggered 10 ns before the signal arrived.

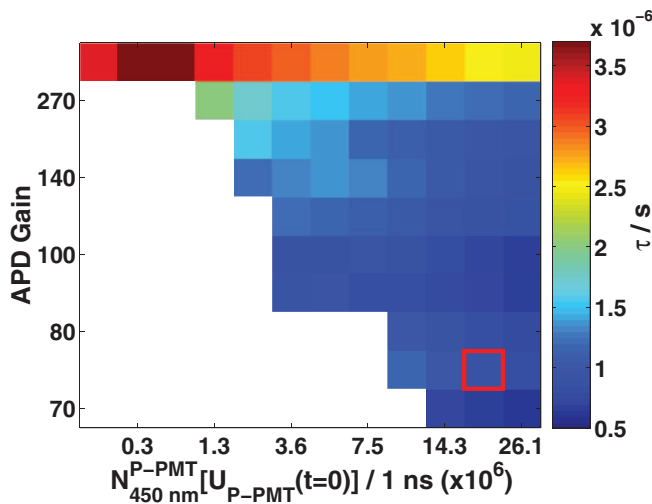


FIG. 16. Response surface of APD at 373 K.

S/N-criteria during evaluation. This is mainly due to the comparatively high transmission losses in the optical fiber coupling. In addition, the moderate gain range accessible for the APD contributed to recorded signal intensities being less than $\frac{1}{2}$ compared to the other detectors. Other than that, the evaluated decay time seems to be stable for the majority of the displayed workspace, except for the row where the gain was highest. This feature at maximum gain appears for all other temperatures that the APD has experienced and indicates that the APD has approached its global gain limit.

In Figure 17 temperature calibration curves for CdWO₄ are plotted, showing evaluated decays for five temperatures from all four detectors under investigation.

Since the decay-time distribution within one response surface can vary to a substantial extent, the points displayed in Figure 17 only describe data from a single fixed matrix element (fixed gain and light intensity). In order to represent a fairly linear part of the workspace as well as having data available for most of the detectors the chosen element corresponds to the second lowest gain at second highest light exposure, i.e., originates from the lower right corner of each surface plot (see red square in Figure 16).

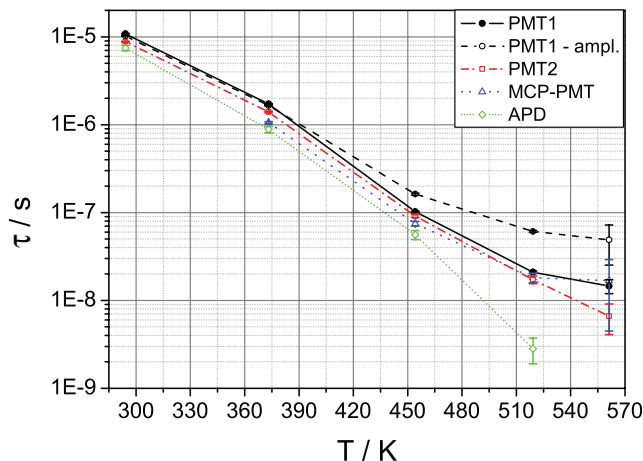


FIG. 17. Temperature calibration points for all detectors from a fixed response matrix element. Error bars indicate one standard deviation from the mean value.

The external amplification of the PMT1 signal shows a systematic effect on the evaluated lifetime. The loss in bandwidth forced the evaluation window to start later in the decay curve at 60 ns compared to the other detectors. This, accompanied with the slight multi-exponential phosphorescence behavior of CdWO₄, accounts for the prolonged decay times that were evaluated here. The result is decreased temperature sensitivity and the inability to measure accurate decays shorter than the signal broadening that is caused by the 5 MHz limited amplifier bandwidth.

For the MCP-PMT the lowest temperature is missing. This is due to the fact that the maximum gate length was restricted to 10 μ s, corresponding to only 1/5 of the sampling time used for the other detectors (see Table II).

The APD proved to exhibit the highest lifetime sensitivity within all investigated detectors. However, the low signal output appeared to be one major restriction leaving no useful data for the highest temperature case.

For clarity, the two operational modes, where the first 10 ns were cut off by time-gating, were omitted. They carried no further relevant information, but were slightly shifted towards longer decays. The change in decay time can be attributed to the slight multi-exponential shape of CdWO₄ phosphorescence accompanied by a fitting window that shifted 10 ns towards a later part of the decay curve.

IV. CONCLUSIONS

Evaluated exponential decays from laser-induced phosphorescence proved to be strongly biased by incoming light intensity, electrical gain and individual properties of each photo detector. It was shown that phosphorescence intensity variations in experiments cannot generally be compensated by adjusting the detector gain without affecting the calculated decay time. Under the investigated operating conditions, the evaluated decay time most commonly varies by a factor of two across an individual response matrix. These response matrices were found to be much more sensitive to nonlinearities than what had been a corresponding signal strength comparison between in- and output (compare Figures 2 and 8). In some cases the maximum decay time can be as much as six times longer than its minimum counterpart for a given temperature (see Figure 15). Clearly, variations of this magnitude add decisive distortions to temperature readings in phosphor thermometry, making detector linearity a key aspect for applications with varying signal intensities. Especially, deviations of signal intensities between calibration and experiment may inflict major systematic temperature errors if detectors are operated outside their linear workspace. Longer decay curves were in general more distorted by gain- and light variations than shorter decay curves at higher temperatures.

All detectors that were involved in this study showed a declining decay-time gradient, visible within the first four intensity columns. The gradient vanished as temperatures rose and the signal decays became shorter. This behavior will be subject for further investigation and is suspected to be phosphor related, as suggested by its gain- and detector independence.

PMT2 (gateable) achieved the best performance amongst all tested devices, providing a large linear workspace without being compromised by additional bandwidth limitations of an external amplifier. Its capability to operate time-gated has not proved its full potential in combination with CdWO₄, but is believed to improve linearity for phosphors that exhibit strong fluorescence peaks along with the phosphorescent decay, as proposed in Ref. 14. The MCP-PMT could only run in time-gated mode and the maximum gate length was limited to 10 μ s, which is a drawback for phosphors with longer decay times. Performing external signal amplification proved to be useful, helping to limit signal saturation in the conventional PMT (PMT1) while maintaining reasonable signal outputs. Its limited bandwidth, however, affected the detection sensitivity for decays, shorter than 200 ns (see Figure 17). The APD's capability to reproduce short decays is superior to any other detector within this comparison study. Nevertheless, signals acquired with the avalanche photodiode exhibited the lowest signal intensities and originated from a very limited gain range. Yet, the former drawback might be of individual nature as the design of the APD's external housing demanded fiber-optical signal collection, accompanied by relatively high coupling losses.

In summary, this study presents a concept of mapping individual detector responses to gain- and light level variations. It can be used for creating a library of decay response curves allowing to correct evaluated decays from measurements performed outside the linear workspace.

ACKNOWLEDGMENTS

This work was financially supported by the HELIOS research project within the European Union's (EU) 7th Framework program for Research and Technical Development/Transportation (Contract No. 030696) and the D60L-2 project financed by the Swedish Energy Agency. The authors would like to acknowledge Ronald Whiddon for helpful discussions.

APPENDIX: DERIVATION AND ERROR ESTIMATION OF N_{λ}^{P-PMT}

This section covers a step-by-step derivation of N_{λ}^{P-PMT} , followed by an error estimation. Figure 4 serves as a starting point indicating that $U_{L-PMT}(t)$ essentially is a Gaussian function with a full width half maximum of around FWHM = 6 ns. It is assumed that $U_{L-PMT}(t)$ is proportional to the optical Power $P(t)$ of the laser pulse, followed by the conclusion that the time integral over $U_{L-PMT}(t)$ can be normalized by a factor f_n to correspond to the laser pulse energy:

$$\begin{aligned} E_{266\text{ ns}}^{\text{pulse}} &= f_n \int_{-\infty}^{\infty} U_{L-PMT}(t) dt \\ &= \int_{-\infty}^{\infty} P(t) dt = \frac{E_{266\text{ ns}}^{\text{pulse}}}{\sigma \sqrt{2\pi}} \int_{-\infty}^{\infty} e^{-\frac{1}{2}(\frac{t}{\sigma})^2} dt. \end{aligned} \quad (\text{A1})$$

In Eq. (A1), σ is the standard deviation and related to the full width half maximum of the Gaussian function by

$$\text{FWHM} = 2\sqrt{\ln 2} \cdot \sigma. \quad (\text{A2})$$

An energy fraction centered on the laser pulse maximum can be described by Eq. (A3) and further simplified if the time window Δt is reasonably small compared to the Gaussian standard deviation σ ,

$$\begin{aligned} E_{266\text{ ns}}^{\Delta t}(t=0) &= \frac{E_{266\text{ ns}}^{\text{pulse}}}{\sigma \sqrt{2\pi}} \int_{-\frac{\Delta t}{2}}^{\frac{\Delta t}{2}} e^{-\frac{1}{2}(\frac{t}{\sigma})^2} dt \\ &\approx \frac{\Delta t \ll \sigma}{\sqrt{2\pi}} \cdot E_{266\text{ ns}}^{\text{pulse}} \cdot \frac{\Delta t}{\sigma}. \end{aligned} \quad (\text{A3})$$

Taking into account the calibration of $U_{L-PMT}(t=0)$ against laser pulse energy from Eq. (1) as well as replacing σ with FWHM using (A2), transforms Eq. (A3) into the following expression:

$$\begin{aligned} E_{266\text{ ns}}^{\Delta t}[U_{L-PMT}(t=0)] \\ \approx 2\sqrt{\frac{\ln 2}{\pi}} \cdot F[U_{L-PMT}(t=0)] \cdot \frac{\Delta t}{\text{FWHM}}. \end{aligned} \quad (\text{A4})$$

The energy area corresponding to (A4) is represented in Figure 4 by the shaded rectangular box. Provided that the energy of one single laser photon can be expressed by $E_{266\text{ nm}}^{\text{photon}} = hc/\lambda_{266\text{ nm}}$, with h representing Planck's constant and c given by the speed of light, Eq. (A4) allows estimating the amount of laser photons $N_{266\text{ nm}}^{\text{phosphor}}$ arriving at the phosphor target within Δt ,

$$\begin{aligned} N_{266\text{ nm}}^{\text{phosphor}}[U_{L-PMT}(t=0)] \\ \approx 2\sqrt{\frac{\ln 2}{\pi}} \cdot \frac{F[U_{L-PMT}(t=0)]}{E_{266\text{ nm}}^{\text{photon}}} \cdot \frac{\Delta t}{\text{FWHM}}. \end{aligned} \quad (\text{A5})$$

In the next step the number of phosphorescence photons N_{λ}^{P-PMT} arriving at the detector within Δt is estimated from the peak voltage $U_{P-PMT}(t=0)$ of the phosphorescence reference PMT. To do so, it is assumed that the phosphor is an isotropic light radiator with both phosphorescence detectors being placed at similar distances. Additionally, collection optics in front of both detectors are required to exhibit identical spectral transmission characteristics. These two assumptions imply that statistically the same amount of phosphorescence photons impinge on both detectors at all times permitting to focus on the P-PMT henceforth. Both reference PMTs (L- and P-) are of identical type and were set to the same constant gain of 6300. However, additional transmission losses have been introduced in front of the L-PMT to keep signal levels comparable to those recorded by the P-PMT reference, see Eq. (A6),

$$T_{L-PMT} = \frac{R_{\text{quartz}}}{T_{\text{quartz}}} \cdot T_{\text{mirror}}^2 \cdot T_{\text{lens}}. \quad (\text{A6})$$

These transmission losses were automatically accounted by the calibration in (1), but have to be considered when comparing peak voltages from both reference detectors. Consequently, a correction as described in (A7) is needed.

$$\begin{aligned} N_{\lambda}^{P-PMT}[U_{P-PMT}(t=0)] \\ = N_{\lambda}^{\text{phosphor}}[U_{P-PMT}(t=0)] \cdot T_{L-PMT}. \end{aligned} \quad (\text{A7})$$

Finally, the spectral radiant sensitivity of the photocathode S_λ (unit: mA/W) needs to be considered since phosphorescence appears red-shifted relative to its laser radiation. For convenience it was previously assumed in (A7) that the phosphorescence wavelength was identical to the laser wavelength such that no wavelength correction was needed as yet. S_λ determines the amount of cathode current I_{cathode} resulting from the transfer of optical power at a given wavelength to the photocathode. The output voltage is related to the cathode current via the load resistance R_{load} and gain as described in Eq. (A8),

$$U_{\text{L/PMT}}(t) = I_{\text{anode}}(t) \cdot R_{\text{load}} = I_{\text{cathode}}(t) \cdot \text{gain} \cdot R_{\text{load}}. \quad (\text{A8})$$

It should be mentioned that in case of saturation the gain factor can be a function of the cathode current and due to accumulation of space charge even be a function of earlier gains and cathode currents. Since the amount of photons, needed for a given cathode current is wavelength dependent, the photon numbers for different wavelengths translate into each other according to Eq. (A9),

$$I_{\text{cathode}} = S_{\lambda_1} \cdot \frac{N_{\lambda_1}}{\Delta t} \cdot E_{\lambda_1}^{\text{photon}} = S_{\lambda_2} \cdot \frac{N_{\lambda_2}}{\Delta t} \cdot E_{\lambda_2}^{\text{photon}} \\ \Rightarrow N_{\lambda_2} = \frac{S_{\lambda_1}}{S_{\lambda_2}} \cdot \frac{E_{\lambda_1}^{\text{photon}}}{E_{\lambda_2}^{\text{photon}}} \cdot N_{\lambda_1}. \quad (\text{A9})$$

Finally, inserting (A5) and (A7) into (A9) provides an estimate for the number of phosphorescence photons arriving at the detector within a time window Δt centered around $t = 0$:

$$N_\lambda^{\text{P-PMT}}[U_{\text{P-PMT}}(t = 0)] \approx \frac{S_{266 \text{ nm}}}{S_\lambda} \cdot 2\sqrt{\frac{\ln 2}{\pi}} \\ \cdot \frac{F[U_{\text{P-PMT}}(t = 0)]}{E_\lambda^{\text{photon}}} \cdot \frac{\Delta t}{\text{FWHM}} \cdot T_{\text{L-PMT}}. \quad (\text{A10})$$

In order to estimate the propagated measurement uncertainty $\Delta N_\lambda^{\text{P-PMT}}$ from (A10) all individual errors (listed in Table III) need to be taken into consideration.

Δt , given by the sampling rate, was assumed to be a fixed value without error. However, the PMT readout voltage is indirectly related to Δt and ΔFWHM , because $\Delta U_{\text{P-PMT}}$ comprises the deviation of the Gaussian from its peak value

TABLE III. Individual error estimates of all quantities in Eq. (A10).

Description	Symbol	Value	Error value	Unit
Radiant cathode sensitivity	$S_{266 \text{ nm}}$	43	1	mA/W
Radiant cathode sensitivity	$S_\lambda (\lambda = 450 \text{ nm})$	53	1	mA/W
Fitting constant from F , Eq. (1)	a	90.0	3.8	μJ
Fitting constant from F , Eq. (1)	b	2.759	3.0×10^{-2}	V^{-1}
P-PMT readout voltage	$U_{\text{P-PMT}}$	Variable	1.26	% (V)
Phosphorescence wavelength	λ	450	34	nm
Photon time window	Δt	1	0	ns
Laser pulse width	FWHM	6	1.15	ns
Optical transmission in front of L-PMT	T_{loss}	9.2	2.1	10^{-8}

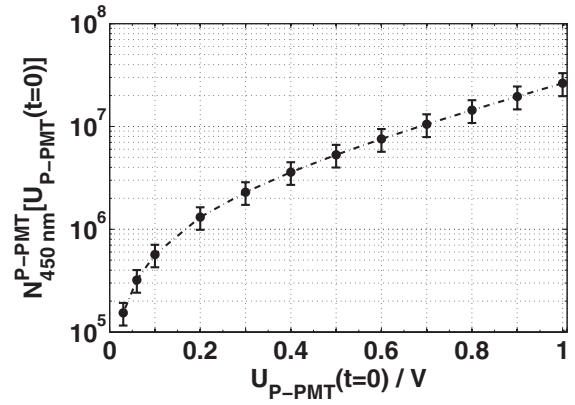


FIG. 18. Photon number as a function of P-PMT peak voltage showing intervals of uncertainty, calculated by Eq. (A11).

within Δt as well as the fact that sampling points are unlikely to hit the exact center of the laser pulse. The latter of these two errors counteracts the former one. The wavelength error $\Delta \lambda$ was given by two standard deviations, assuming that the spectral bandpass filter has a Gaussian spectral transmittance with FWHM = 40 nm. Certainly, ΔT_{loss} has the biggest impact on measurement uncertainty (see Table III). Its value has been calculated by propagating uncertainties from individual transmission objects, listed in Eq. (A6). The reason for ΔT_{loss} being in the order of 23% can be attributed mainly to the two mirror transmissions, each having a relative uncertainty of around 10% due to their very low transmission value of around $T_{\text{mirror}} = 1.875 \times 10^{-3}$. The total measurement uncertainty is described by Eq. (A11) and has been plotted in Figure 18 using the values from Table III,

$$\Delta N_\lambda^{\text{P-PMT}} = N_\lambda^{\text{P-PMT}} \cdot \left[\left(\frac{\Delta S_{266 \text{ nm}}}{S_{266 \text{ nm}}} \right)^2 + \left(\frac{\Delta S_\lambda}{S_\lambda} \right)^2 \right. \\ \left. + \left(\frac{\Delta \text{FWHM}}{\text{FWHM}} \right)^2 + \left(\frac{\Delta \lambda}{\lambda} \right)^2 + \left(\frac{\Delta T_{\text{L-PMT}}}{T_{\text{L-PMT}}} \right)^2 \right. \\ \left. + \left(\frac{\Delta a}{a} \right) + \left(1 + \frac{a}{F} \right)^2 \right. \\ \left. \cdot (\Delta b^2 \cdot U_{\text{P-PMT}}^2 + \Delta U_{\text{P-PMT}}^2 \cdot b^2)^2 \right]^{\frac{1}{2}}. \quad (\text{A11})$$

Figure 18 displays the number of photons calculated as a function of $U_{\text{P-PMT}}(t = 0)$ together with the measurement uncertainty to be seen as error bars. Measurement points have been chosen to match the photon axis from all response surface plots.

¹S. W. Allison and G. T. Gillies *Rev. Sci. Instrum.* **68**, 2615 (1997).

²A. H. Khalid and K. Kontis, *Sensors* **8**(9), 5673 (2008).

³M. Aldén, A. Omrane, M. Richter, and G. Särner, *Prog. Energy Combust. Sci.* **37**(4), 422 (2011).

⁴A. Omrane, F. Ossler, and M. Aldén, *Proc. Combust. Inst.* **29**, 2653 (2002).

⁵T. Kissel, E. Baum, A. Dreizler, and J. Brübach, *Appl. Phys. B* **96**, 731 (2009).

⁶Y. R. Chen and K. L. Bray, *Phys. Rev. B* **56**, 10882 (1997).

- ⁷J. Brübach, A. Dreizler, and J. Janicka, *Meas. Sci. Technol.* **18**, 764 (2007).
- ⁸S. W. Allison, D. L. Beshears, T. Bencic, W. A. Hollerman, and P. Boudreaux, "Development of temperature-sensitive paints for high temperature aeropropulsion applications," AIAA Paper No. 2001-3528, 2001.
- ⁹R. M. Ranson, C. B. Thomas, and M. R. Craven, *Meas. Sci. Technol.* **9**, 1947 (1998).
- ¹⁰J. Brübach, J. P. Feist, and A. Dreizler, *Meas. Sci. Technol.* **19**, 025602 (2008).
- ¹¹C. Knappe, P. Andersson, M. Algotsson, M. Richter, J. Lindén, M. Aldén, M. Tunér, and B. Johansson, *SAE Int. J. Engines* **4**, 1689 (2011).
- ¹²J. R. Lakowicz, *Principles of Fluorescence Spectroscopy* (Springer Science + Business Media, New York, 2006), p. 141.
- ¹³J. Lindén, C. Knappe, M. Richter, and M. Aldén, *Meas. Sci. Technol.* **23**, 035201 (2012).
- ¹⁴C. Knappe, J. Lindén, F. Abou Nada, M. Richter, and M. Aldén, *Rev. Sci. Instrum.* **83**, 034901 (2012).
- ¹⁵See http://sales.hamamatsu.com/assets/pdf/parts_H/H6780-04.pdf for H6780-04 PMT Datasheet.
- ¹⁶R. W. Engstrom, *J. Opt. Soc. Am.* **37**, 420 (1947).
- ¹⁷D. H. Hartman, *Rev. Sci. Instrum.* **49**, 1130 (1978).
- ¹⁸H. Kunz, *Metrologia* **5**, 88 (1969).